Comparison and Optimization of Burnishing Parameters in Various Machining Conditions

Trung-Thanh Nguyen[1] – Minh-Thai Le[2] – Thai-Chung Nguyen[1] – Truong-An Nguyen[1] – Xuan-Ba Dang[3] – An-Le Van[4, ✉]

1 Le Quy Don Technical University, Faculty of Mechanical Engineering, Vietnam
2 Le Quy Don Technical University, Faculty of Special Equipment, Vietnam
3 Ho Chi Minh City University of Technology and Education, Vietnam
4 Nguyen Tat Thanh University, Faculty of Engineering and Technology, Vietnam

✉ lvan@ntt.edu.vn

Abstract   This study proposes a cryogenic diamond burnishing process and optimizes cooling parameters, including the distance to nozzle (N), nozzle diameter (D), and CO_2 flow rate (Q) to minimize the maximum roughness (R), energy consumption (E), and circularity (C). The Kriging and adaptive-network-based fuzzy inference system (ANFIS) methods were ultilized to propose the response models. The CRITIC, non-dominated sorting genetic algorithm-II (NSGA-II), and MABAC were applied to calculate the weights, generate feasible solutions, and select the best optimal data. The result indicated that the optimal N, D, and Q were 15 mm, 9 mm, and 8 L/min, respectively. The reductions in the roughness, energy, and circularity were 15.5 %, 2.0 %, and 38.6 %, respectively. The roughness and energy models were primarily affected by Q, D, and N, respectively, while circularity model was influenced by the N, D, and Q, respectively. The proposed process could be used to machine different holes with minimizing environmental impacts. Lower roughness and circularity were achieved using the cryogenic diamond burnishing process. The Kriging-NSGA-II could be utilized to show non-linear data and produce the best results.

Keywords   cryogenic diamond burnishing; energy consumption; maximum roughness; circularity; Kriging model

Highlights
- *A cryogenic CO_2 diamond burnishing process is proposed and optimized.*
- *Minimizing the maximum surface roughness, energy, and circularity.*
- *The Kriging and ANFIS approaches are employed to develop the predictive models.*
- *The reductions in the R, E, and C were 15.5 %, 2.0 %, and 38.6 %, respectively.*

1 INTRODUCTION

Cryogenic cooling is an approach to cool workpieces and tools quickly and effectively in which refrigerants, such as liquid nitrogen or solid carbon dioxide, are used directly. This method has several advantages, including cost-effectiveness, faster cooling, improved tool life, better surface finish, and higher productivity. The cryogenic method has great potential to replace conventional cooling strategies in consideration of machinability.

The applications of cryogenic cooling on different burnishing operations have been extensively considered. Caudill et al. [1] presented that the roughness, hardness, and depth of the affected layer of the cryogenic burnished Ti-6Al-4V improved by 56.7 %, 64.2 %, and 25.2 %, respectively, compared to the dry condition. The temperature in the cryogenic burnishing operation of Co-Cr-Mo biomedical alloy was reduced by 50 %, while the depth of the affected layer was increased by 150 %, compared to the dry condition [2]. Yang et al. [3] emphasized that cryogenic cooling could be used to obtain a higher depth of the affected layer, increased micro-hardness, and fine grain size, compared to the base material. Huang et al. [4] presented those higher tangential forces and lower temperatures are observed from a cryogenic burnishing Al 7050-T7451. Tang et al. [5] indicated that the cryogenic conditions facilitated to produce the corrosion film on the subsurface layer of the Ti-6Al-4V. Similarly, a low roughness and nanocrystalline layer on the burnished Ti-6Al-4V titanium alloy was produced with the aid of cryogenic burnishing [6]. A set of experiments was conducted to reduce the roughness and improve the hardness of the burnished 17-4 PH stainless steel [7]. The authors stated that the roughness of 0.03 µm and hardness

of 413 HV could be generated at the optimal solution. The optimal burnishing force, feed, and speed of the machined 17-4 PH stainless steel were selected using the desirability approach [8]. The outcomes presented that a roughness of 0.20 µm and a hardness of 397.48 HV were achieved. Rotella et al. [9] presented that the wear resistance of the burnished Ti6Al4V titanium alloy was enhanced by 86.2 % with the aid of cryogenic cooling and coated tools. The regression models of the roughness, hardness, wear rate, and the depth of the affected layer were developed for the cryogenic burnishing Ti-6Al-4V alloy [10]. The small errors between models and experiments indicated that the developed models were adequate. Sachin et al. [11] presented that the roughness was reduced when higher values of speed, feed, and force were employed. Caudill et al. [12] presented that cryogenic cooling increased the yield strength and produced nanostructured layer of the burnished Ti-6Al-4V. Huang et al. [13] emphasized that the surface hardness of the cryogenic burnished Al 7050-T7451 could be increased by 29.8 %. Maximov et al. [14] presented that the roughness of the burnished stainless steel could be changed from 0.041 to 0.049 µm using a cryogenic condition. Van and Nguyen stated that roughness and energy of the cold air-based burnishing process were reduced by 34.1 % and 1.5 %, respectively, while the power factor and Vickers hardness improved by 13.2 % and 9.5 %, at the selected solution [15]. Maximov stated that the fatigue strength of the cryogenic-burnished SS304 was improved by 36.4 %, compared to the untreated specimen [16].

However, an internal diamond burnishing process using the liquid CO_2 has not been developed and optimized. The impacts of the liquid CO2, including the distance to the nozzle, nozzle diameter, and flow rate on the roughness, energy, and hole circularity have not

been investigated. Finally, a multi-response optimization has not been performed to reduce energy as well as roughness and improve circularity.

The following section presents the optimization strategy. After that, the experimental setup and results are explained. Lastly, some conclusions are made.

2 METHODS AND MATERIALS

2.1 Optimizing Framework

In this study, the roughness (R) is calculated as:

$$R = \frac{\sum_{i=1}^{3} Sz_i}{3},\tag{1}$$

where Sz_i is the maximum height of the scale limited surface roughness. The energy consumption (E) is calculated as:

$$E = P_m \times t_m,\tag{2}$$

where P_m and t_m denote the burnishing power and burnishing duration, respectively. The circularity (C) is calculated as:

$$C = \frac{\sum_{i=1}^{3} CC_i}{3},\tag{3}$$

where CC_i is the circularity of the burnished hole.

The parameters and their levels, including the distance to the nozzle, nozzle diameter, and CO_2 flow rate are shown in Table 1. The flow rate is selected using the properties of the valve and CO_2 storage equipment. The distance to nozzle and nozzle diameter are referenced from related publications and experts in the brunishing field.

The optimizing procedure for the burnishing process is illustrated in Fig. 1. In this work, the advantages of various methods (Kriging, ANFIS, CRITIC, NSGA-II, and MABAC) were combined to propose the optimization approach.

Step 1: Executing 27 trials using the full factorial method [17-20].

Step 2: The CRITIC is used to compute the weights of the responses [21]. The response (f_{ij}) is normalized as:

$$f_{ij} = \frac{x_{ij} - x_{worst}}{x_{best} - x_{worst}},\tag{4}$$

where x_{best} and x_{worst} are the best and worst values of each response, respectively. The standard deviation (s_j) is calculated as:

$$s_j = \sqrt{\frac{(\sum_{i=1}^{m} f_{ij} - x_m)^2}{m-1}}.\tag{5}$$

The conflict (I_j) among criteria is calculated as:

$$I_j = \sum_{k=1}^{m} (1 - r_{jk}),\tag{6}$$

where r_{jk} is the correlation coefficient between the vectors x_j and x_k. The quantity (C_j) is calculated as:

$$C_j = s_j \sum_{k=1}^{m} (1 - r_{jk}).\tag{7}$$

The computed (ω_i) is calculated as:

$$\omega_i = \frac{C_j}{\sum_{k=1}^{n} C_j}.\tag{8}$$

Step 3: The Kriging approach is used to construct the predictive models of the responses [22-25]. The Kriging model is expressed as:

$$f(x) = f^T(x)\beta + r^T(x)R^{-1}(Y - F\beta),\tag{9}$$

where β denotes the least-squares estimate, and Y presents the true responses at the sample. The log-likelihood of the model parameters is expressed as:

$$\ln\left(u', \widehat{\sigma}^2, \theta\right) = -\frac{n}{2}\ln(2\pi) - \frac{n}{2}\ln\left(\widehat{\sigma}^2\right) - \frac{1}{2}\ln(|R|)$$
$$- \frac{1}{2\widehat{\sigma}^2}(Y - F\beta)' R^{-1}(Y - F\beta).\tag{10}$$

The σ^2 is estimated as:

$$\widehat{\sigma}^2 = \frac{1}{n}(Y - F\widehat{\beta})^T R^{-1}(Y - F\widehat{\beta}).\tag{11}$$

Step 4: The R, E, and C models are proposed using the ANFIS approach [26-29].

Layer I: The outputs of R, E, and C responses are expressed as:

$$R(x) = \mu_E A_1 x(R),\tag{12}$$

$$E(y) = \mu_T A_2 y(E),\tag{13}$$

$$C(z) = \mu_D A_3 z(C),\tag{14}$$

where A_i is the connected label of each response.

Layer II: The fixed function is expressed as:

$$L_2, x = \mu_E A_1 x(R) \times \mu_T A_2 y(E) \times \mu_D A_3 z(C).\tag{15}$$

Layer III: The firing strength is expressed as:

$$L_3, x = \overline{w_i} = \frac{w_i}{\sum_{i=1}^{n} w_i},\tag{16}$$

Layer IV: The output is expressed as:

$$L_4, x = \overline{w_i} f_i(x) = \overline{w_i}(g_i x + h_i x + k_i),\tag{17}$$

where g_i, h_i, and k_i are the consequent parameters, respectively.

Layer V: The fixed node is expressed as:

$$L_5, x = \sum_i \overline{w_i} f_i.\tag{18}$$

Step 5: The selection of the optimality using the NSGA-II and MABAC. The operating principle of the NSGA-II is expressed as [30-33]. An initial population P_0 of size N is randomly generated at the start of the procedure.

The non-domination ranks and crowding distance are used to evaluate each individual. The crowding distance among individuals is computed as:

$$d_j = \sum_{m=1}^{M} \frac{f_m^{\max j+1} - f_m^{\min j-1}}{f_m^{\max} - f_m^{\min}},\tag{19}$$

where f_m is the mth objective function. The parent-offspring generation is produced in the crossover operation. The arithmetic crossover function is expressed as:

$$S_i = 0.5(1 + \gamma)P_i + 0.5(1 - \gamma)P_{i+1},\tag{20}$$

where S and P are the off spring and parent, respectively, and γ is a crossover coefficient. The mutation operation is used to produce the individual diversity and expressed as:

$$S = \begin{cases} S + (2r)^{1/n_m + 1} - 1, & \text{if } r \le 0.5 \\ S + 1 - (2 - 2r)^{1/n_m + 1} & \text{else} \end{cases}.\tag{21}$$

The MABAC is expressed as [34]. The weighted response (v_{ij}) is calculated as:

$$v_{ij} = \omega_j(n_{ij} + 1),\tag{22}$$

where n_{ij} is the normalized response. The approximation area (g_i is calculated as:

$$g_i = (\prod_{j=1}^{m} v_{ij})^{1/m}.\tag{23}$$

The alternative distance (d_{ij}) is calculated as:

$$d_{ij} = v_{ij} - g_i.\tag{24}$$

The performance index (P_i) is calculated as:

$$P_i = \sum_{j=1}^{n} d_{ij}.$$ (25)

The best solution is selected with the highest P_i.

Table 1. Process parameters of the burnishing operation

Parameters	Levels
Distance to the nozzle, N [mm]	15-25-35
Nozzle diameter, D [mm]	6-8-10
CO2 flow rate, Q [L/min]	4-8-12

2.1 Experimental Facilities

The experiments are performed with the aid of a NC lathe (Fig. 2). The EN24 steel is applied to produce the high-strength shafts, punches, dies, bushings, rings, and gears. The workpiece with a length of 64 mm, an internal diameter of 44 mm, and an external diameter of 58 mm is used. The pre-machined surface is generated using the drilling and turning operations. The roughness and circularity of the initial surface are 14.034 μm and 50.63 μm, respectively.
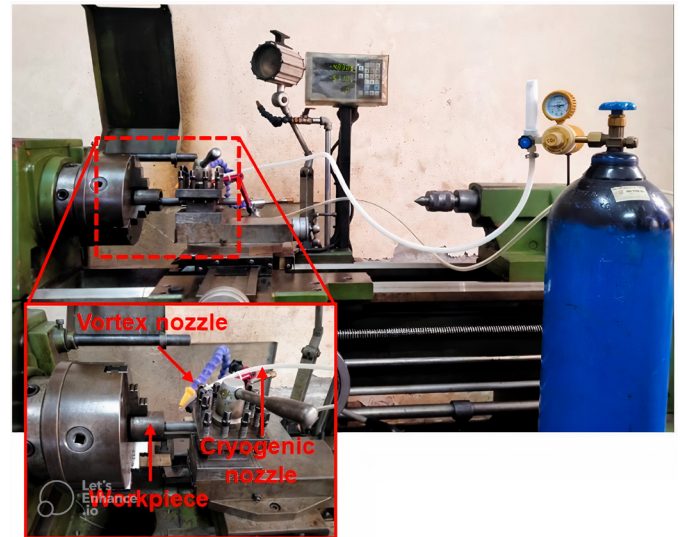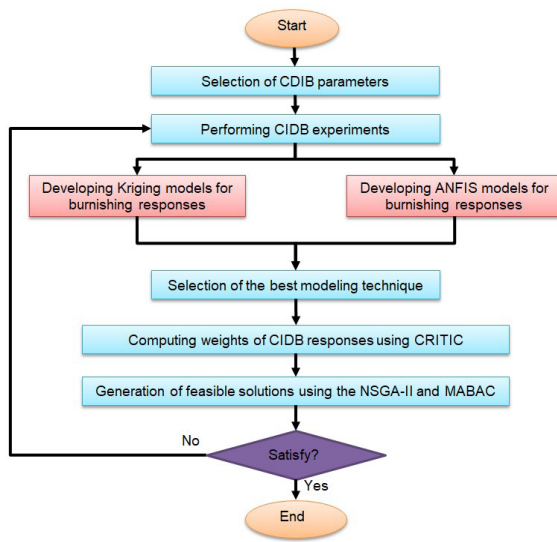

Fig. 2. Experimental burnishing

The roughness, power, and circularity are measured using the ZeGage Pro-3D, Kyoritsu 6315, and ZEISS CONTURA CMM, respectively. The roughness is measured in three different points of the burnished surface. The power is captured from ten peak values of the obtained data. The circularity is measured at 8 positions at various circular cross-sections, and the average value is then determined (Fig. 3c). The experimental outcomes at various burnishing conditions are presented in Fig. 3.

Fig. 1. Optimization approach

3 RESULTS AND DISCUSSIONS

3.1 Comparing Responses in Various Conditions

The experimental data are shown in Table 2. To prove the effectiveness of the proposed process, a set of experiments is conducted in dry, wet, and cryogenic conditions. The comparative results for the roughness are shown in Fig. 4. Quantitatively, the cryogenic CO_2 reduces the roughness from 28.82 % to 34.42 %, compared to the dry environment. Similarly, the cryogenic CO_2
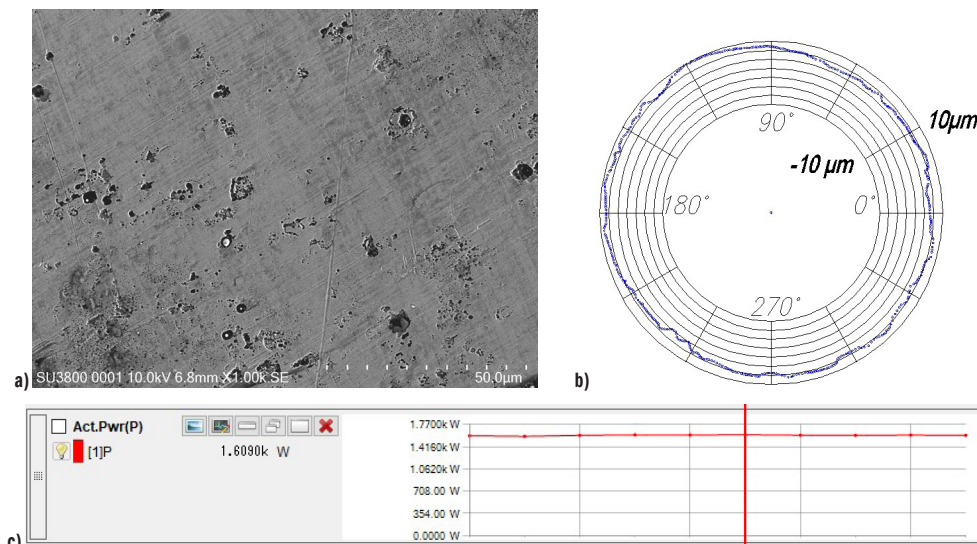

Fig. 3. Example results of the burnishing process at the experimental No. 6; SEM image, b) circularity, and c) power consumed

reduces the roughness from 13.03 % to 17.11 %, compared to the wet environment. Greater roughness occurs under dry conditions due to inadequate heat dissipation from the workpiece surface. The liquid CO_2 effectively removes the temperature and friction at the interfaces due to thin-film lubrication, resulting in low roughness.

Table 2. Experimental results

No.	N [mm]	D [mm]	Q [L/min]	R [μm]	E [kJ]	C [μm]
		Experimental data for developing models				
1	15	6	4	4.226	60.14	19.46
2	25	6	4	4.508	64.72	22.31
3	35	6	4	5.031	67.52	27.67
4	15	6	8	3.725	65.87	14.73
5	25	6	8	3.992	69.97	17.25
6	35	6	8	4.497	72.26	22.28
7	15	6	12	3.549	70.04	12.89
8	25	6	12	3.797	73.61	15.07
9	35	6	12	4.286	75.42	19.76
10	15	8	4	3.873	65.14	13.51
11	25	8	4	4.181	69.37	16.77
12	35	8	4	4.731	71.79	22.54
13	15	8	8	3.151	70.66	9.31
14	25	8	8	3.442	74.42	12.22
15	35	8	8	3.974	76.34	17.66
16	15	8	12	2.754	74.58	7.97
17	25	8	12	3.028	77.83	10.55
18	35	8	12	3.543	79.28	15.65
19	15	10	4	3.746	69.51	10.26
20	25	10	4	4.079	73.38	13.93
21	35	10	4	4.654	75.45	20.11
22	15	10	8	2.803	74.82	6.55
23	25	10	8	3.119	78.26	9.89
24	35	10	8	3.677	79.78	15.74
25	15	10	12	2.185	78.52	5.73
26	25	10	12	2.484	81.41	8.73
27	35	10	12	3.025	82.51	14.24
		Experimental data for testing models				
28	20	7	5	3.953	66.64	15.93
29	20	9	7	3.251	73.68	9.62
30	18	7	9	3.365	70.83	11.54
31	22	9	10	2.836	77.43	8.51
32	26	7	11	3.469	75.32	13.07
33	30	9	5	4.108	74.12	16.32
34	32	7	10	3.828	75.73	16.36
35	16	9	9	2.811	74.35	7.24
36	34	9	11	3.297	80.36	14.12
37	24	7	8	3.649	71.95	14.01

The comparative results for the circularity are shown in Fig. 5. Quantitatively, cryogenic CO_2 reduces the circularity from 29.47 % to 32.17 %, compared to the dry environment. Similarly, cryogenic CO_2 reduces the circularity from 16.11 % to 19.18 %, compared to the wet environment. The liquid CO_2 enhances the cooling efficiency, leading to even deformation of the burnished hole; thus the circularity reduces.

3.2 The Selection of a Better Modelling Technique

The comparisons between the actual and predcitve data of the Kriging and ANFIS models are shown in Tables 3 and 4, respectively. For the

Kriging model, the errors of the roughness, energy, and circularity lie from –0.63 % to 0.39 %, –0.72 % to 0.42 %, and –1.10 % to 0.78 % respectively. For the ANFIS model, the errors of the roughness, energy, and circularity lie from –3.30 % to 2.36 %, –1.61 % to 4.45 %, and –5.78 % to 5.43 %, respectively. As compared to the models produced by the ANFIS approach, the predictive data generated by the Kriging method have a stronger association with the experimental data.
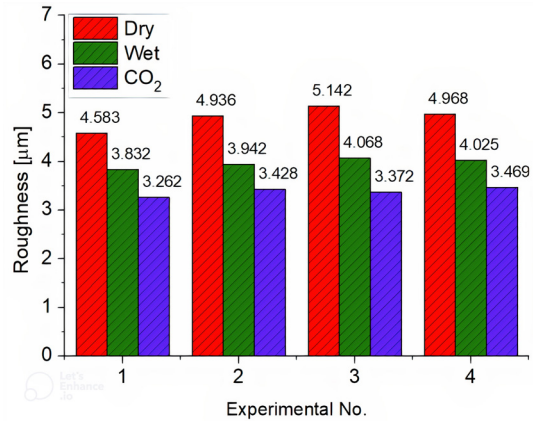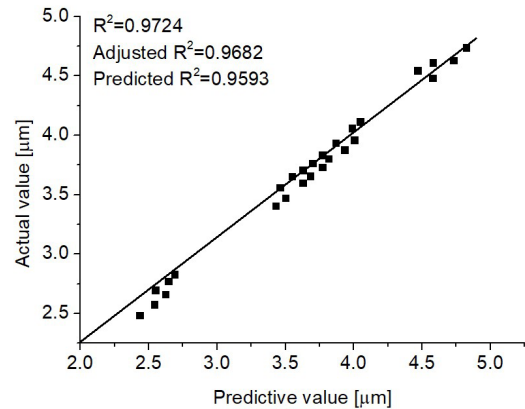

Fig. 4. Comparative roughness

Fig. 5. Comparative circularity

Fig. 6 presents the consistent data of the burnishing responses; thus the developed Kriging models are adequate.

3.3 ANOVA Analysis for Burnishing Responses

The computed ANOVA results for the roughness, energy, and circularity are presented in Tables 5-7, respectively. The F-values of the roughness, energy, and circularity models are 27.42, 61.59, and 26.80, respectively, indicating their significance. For the roughness model, the Q has the highest contributions (21.35 %), followed by the D (20.76 %) and N (16.96 %), respectively. The contributions of the ND, NQ, and DQ are 6.43 %, 7.52 %, and 4.67 %, respectively. The contributions of the N^2, D^2, and Q^2 are 7.04 %, 7.62 %, and 7.65 %, respectively. For the energy model, the contributions of the N, D, and Q are 19.92 %, 28.87 %, and 29.28 %, respectively. The contributions of the ND, NQ, and DQ are 2.52 %, 3.42 %, and 1.92 %, respectively. The contributions of the N^2, D^2, and Q^2 are 6.323 %, 2.21 %, and 5.63 %, respectively. For the circularity model, the contributions of the N, D, and Q are 25.69 %, 22.61 %, and 19.11 %, respectively. The contributions of the ND, NQ, and DQ are 2.51 %, 2.07 %, and 3.13 %, respectively. The contributions of the N^2, D^2, and Q^2 are 7.71 %, 8.28 %, and 8.85 %, respectively.

Table 3. Testing results for developed Kriging models

No.	R [μm]			E [kJ]			C [μm]		
	Exp.	Kri.	Er. [%]	Exp.	Kri.	Er. [%]	Exp.	Kri.	Er. [%]
28	3.953	3.967	−0.35	66.64	66.52	0.18	15.93	15.82	0.69
29	3.251	3.267	−0.49	73.68	73.52	0.22	9.62	9.71	−0.94
30	3.365	3.354	0.33	70.83	70.53	0.42	11.54	11.45	0.78
31	2.836	2.854	−0.63	77.43	77.86	−0.56	8.51	8.58	−0.82
32	3.469	3.456	0.37	75.32	75.02	0.40	13.07	13.14	−0.54
33	4.108	4.113	−0.12	74.12	74.65	−0.72	16.32	16.25	0.43
34	3.828	3.842	−0.37	75.73	75.92	−0.25	16.36	16.48	−0.73
35	2.811	2.824	−0.46	74.35	74.56	−0.28	7.24	7.32	−1.10
36	3.297	3.284	0.39	80.36	80.48	−0.15	14.12	14.18	−0.42
37	3.649	3.662	−0.36	71.95	71.76	0.26	14.01	14.09	−0.57

Table 4. Testing results for ANFIS models

No.	R [μm]			E [kJ]			C [μm]		
	Exp.	Kri.	Er. [%]	Exp.	Kri.	Er. [%]	Exp.	Kri.	Er. [%]
28	3.953	3.842	2.81	66.64	65.23	2.12	15.93	16.85	−5.78
29	3.251	3.362	−3.41	73.68	74.02	−0.46	9.62	9.84	−2.29
30	3.365	3.402	−1.10	70.83	69.32	2.13	11.54	11.96	−3.64
31	2.836	2.964	−4.51	77.43	78.64	−1.56	8.51	8.96	−5.29
32	3.469	3.365	3.30	75.32	74.25	1.42	13.07	12.36	5.43
33	4.108	4.196	−2.14	74.12	73.21	1.23	16.32	16.94	−3.80
34	3.828	3.901	−1.91	75.73	72.36	4.45	16.36	15.86	3.06
35	2.811	2.765	1.64	74.35	75.03	−0.91	7.24	7.56	−4.42
36	3.297	3.152	4.40	80.36	81.65	−1.61	14.12	14.63	−3.61
37	3.649	3.552	2.66	71.95	72.86	−1.26	14.01	13.56	3.21

Table 5. ANOVA results for the roughness model

So	SS	MS	F value	p-value
Model	5.8247	0.6472	27.42	<0.0001
N	12.8611	12.8611	544.96	<0.0001
D	15.7427	15.7427	667.06	<0.0001
Q	16.1901	16.1901	686.02	<0.0001
ND	4.8760	4.8760	206.61	<0.0001
NQ	5.7025	5.7025	241.63	<0.0001
DQ	3.5413	3.5413	150.06	0.0006
N^2	5.3386	5.3386	226.21	<0.0001
D^2	5.7784	5.7784	244.85	<0.0001
Q^2	5.8011	5.8011	245.81	<0.0001
Res.	0.1653	0.0236		
Cor.	5.99			
$R^2 = 0.9724$; Adjusted $R^2 = 0.9682$; Predicted $R^2 = 0.9593$				

Table 6. ANOVA results for the energy model

So	SS	MS	F value	p-value
Model	19509.10	1393.51	49.50505051	<0.0001
N	321.51	35.72	61.59	<0.0001
D	70.00	70.00	120.69	<0.0001
Q	101.45	101.45	174.92	<0.0001
ND	102.89	102.89	177.40	<0.0001
NQ	8.86	8.86	15.27	0.0011
DQ	12.02	12.02	20.72	0.0006
N^2	6.75	6.75	11.63	0.0015
D^2	21.89	21.89	37.75	0.0003
Q^2	7.77	7.77	13.39	0.0009
Res.	4.07	0.58		
Cor.	325.58			
$R^2 = 0.9875$; Adjusted $R^2 = 0.9802$; Predicted $R^2 = 0.9786$				

3.4 The Impacts of Cooling Parameters on the Roughness, Energy, and Circularity

The main impacts of process parameters on the roughness are shown in Fig. 7. A higher N increases the friction at the burnishing area due to lower cooling effects; thus a higher roughness is produced. A higher D increases the cooling efficiency at the interfaces. The friction and temperature decrease; results in a lower roughness. As depicted in an increased Q leads to a higher CO_2 intensity, leading to reductions in friction and temperature; thus this reduces the roughness.
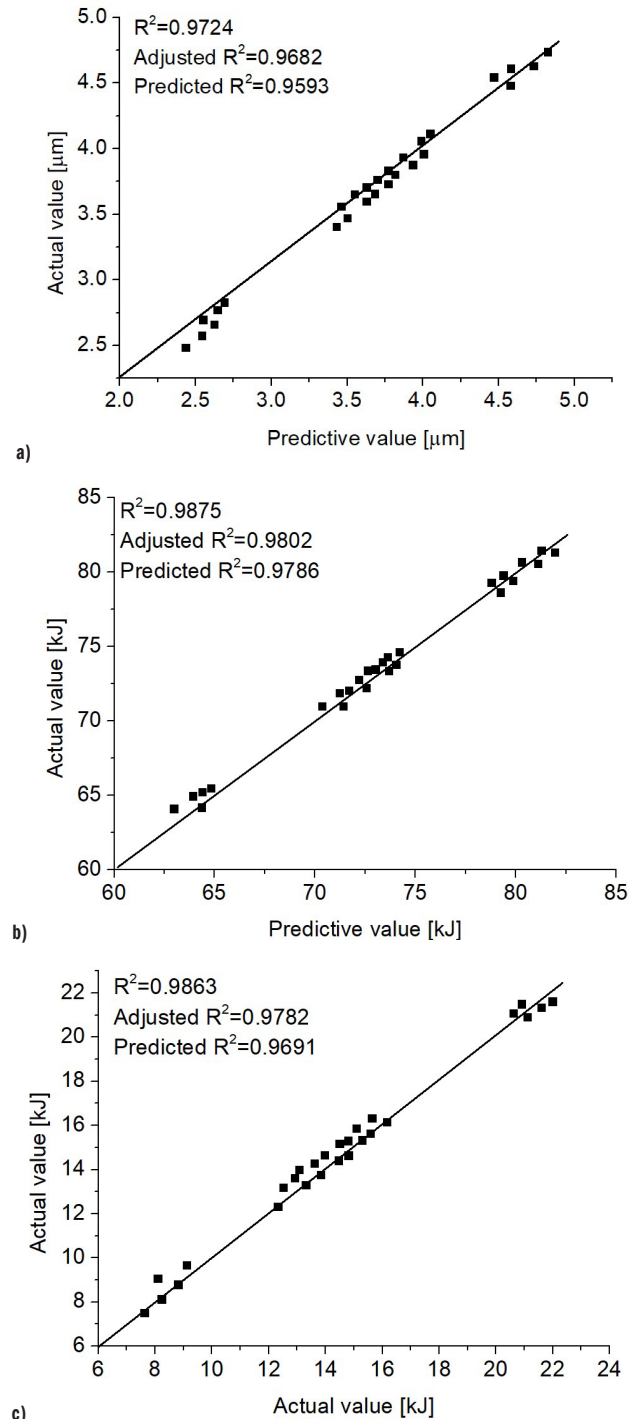
a)

b)

c)

Fig. 6. Comparisons between the predictive and actual values; a) roughness model, b) energy model, and c) circularity model

The main impacts of parameters on the energy are shown in Fig. 8. A higher N causes higher friction at the machining region; thus a higher energy is required to overcome a greater load. A higher D increases the amount of the CO_2 and the workpiece hardness increases; thus a higher energy is required. An increased Q leads to a higher CO_2 intensity, leading to higher workpiece hardness; thus a higher energy is used to overcome a greater resistance.

The main impacts of parameters on the circularity are shown in Fig. 9. A higher N increases friction at the interface, resulting in hard compression of material; thus the circularity increases. A higher D increases cooling efficiency due to higher liquid CO_2 quantity. The friction decreases, leading to even deformation of the material compression; thus the circularity reduces. An increased Q leads to a higher CO_2 intensity, leading to reductions in friction at the burnishing region. The material compression evenly is produced; thus the circularity reduces.

3.5 The Impacts of Cooling Parameters on the Microstructure

The microstructure of the burnished specimen under various parameters is presented in Fig. 10. When the N increases from 15 mm to 35 mm, the Vickers hardness and the depth reduce from
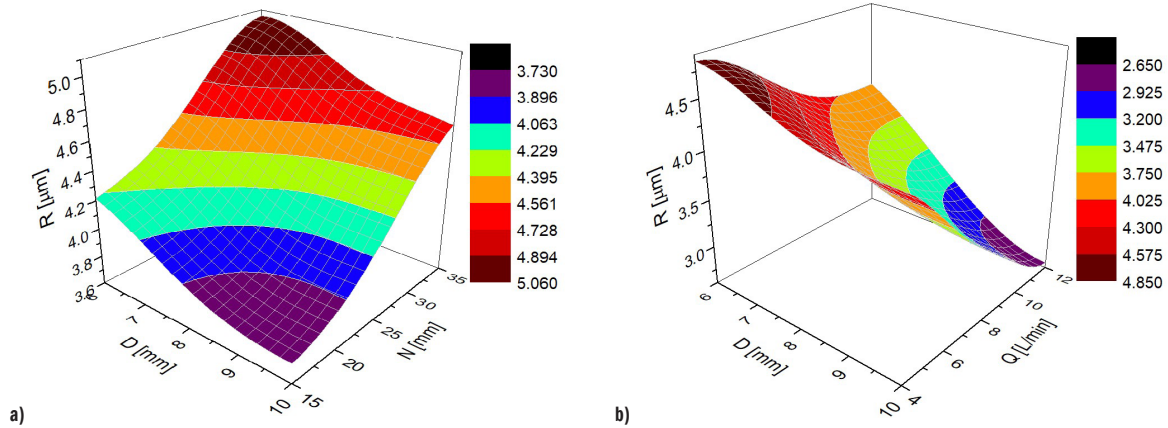

Fig. 7. Kriging plots for the roughness model; a) R vs. N and D, and b) R vs. Q and D
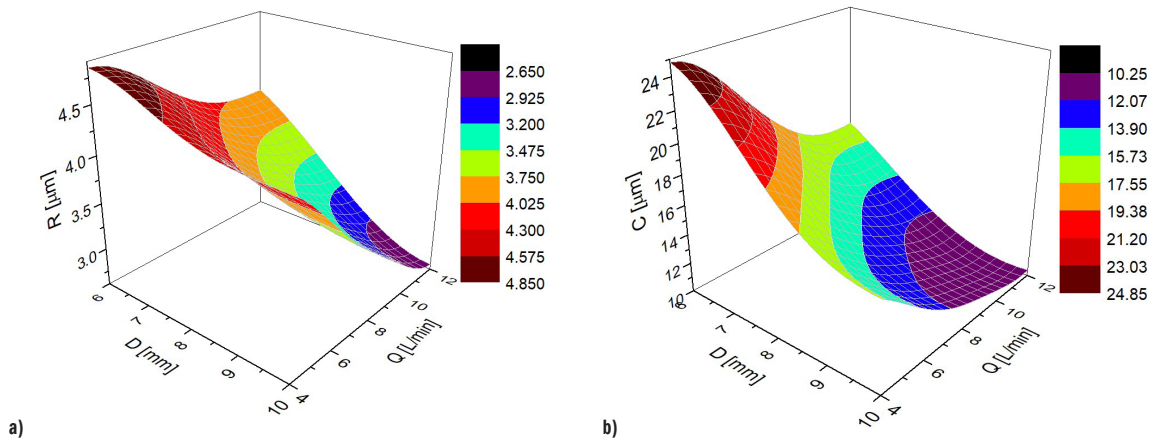

Fig. 8. Kriging plots for the energy model; a) E vs. N and D, and b) E vs. Q and D
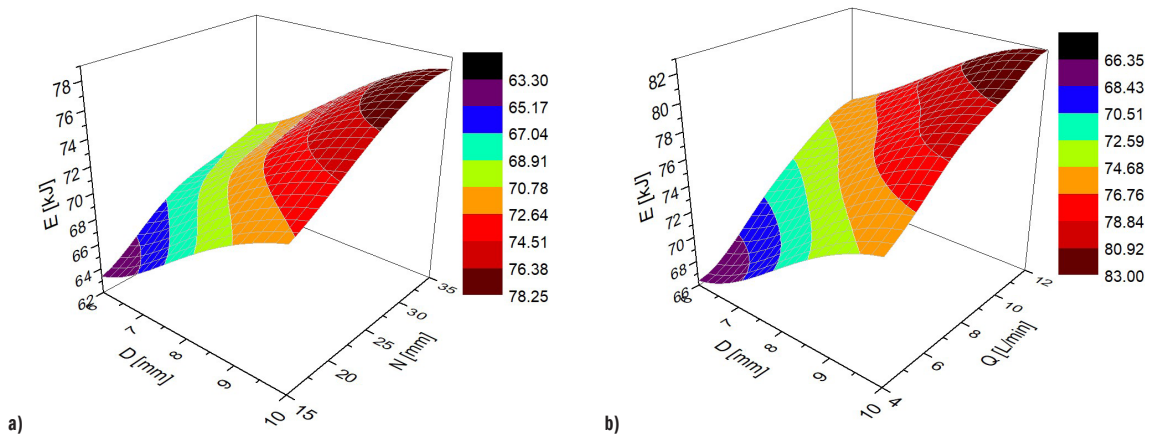

Fig. 9. Kriging plots for the circularity model; a) C vs. N and D, and b) C versus Q and D
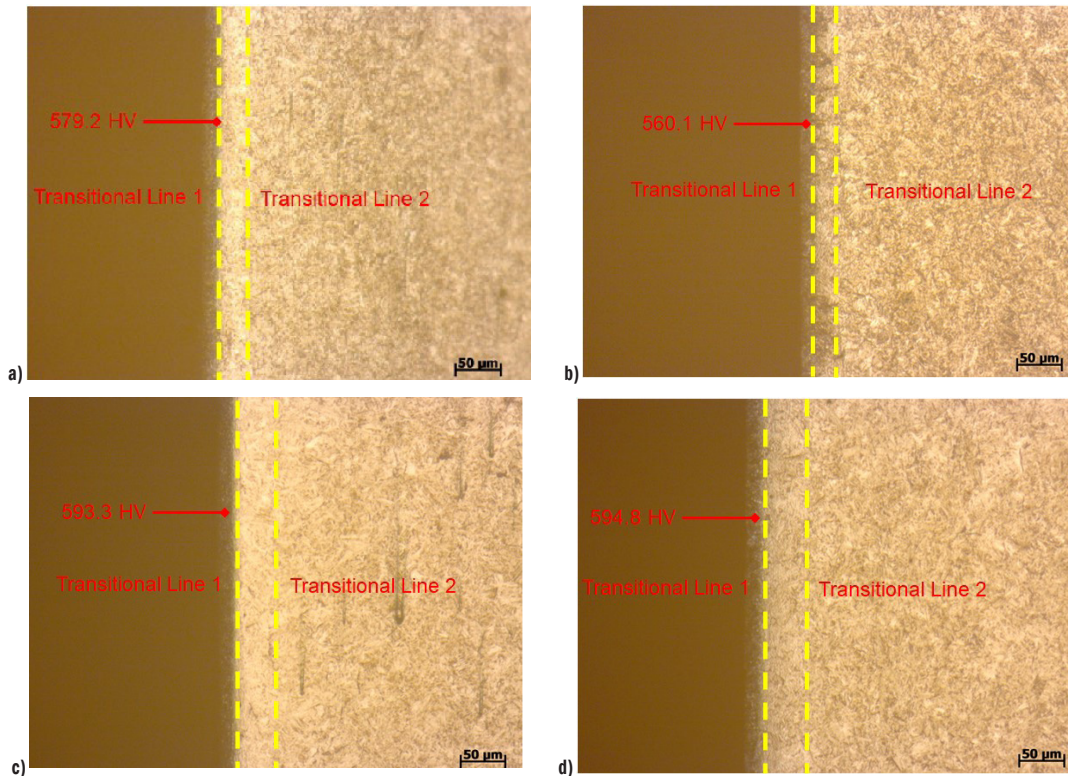
Fig. 10. The impacts of the cooling parameters on the microstructure; a) N = 15 mm, D = 6 mm, Q = 8 L/min, b) N = 35 mm, D = 6 mm, Q = 8 L/min, c) N = 15 mm, D = 10 mm, Q = 8 L/min, and d) N = 15 mm, D = 6 mm, Q = 12 L/min
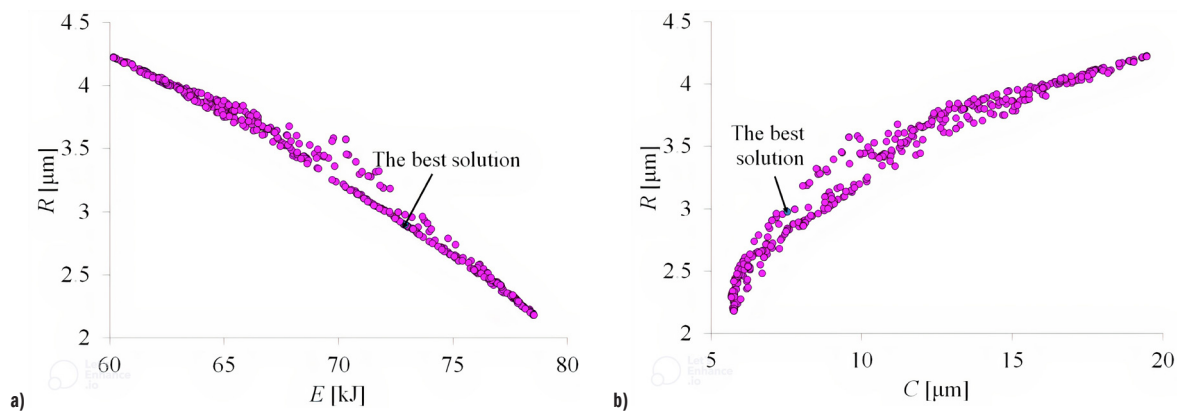

Fig. 11. Pareto fronts generated by NSGA- II; a) roughness and energy, and b) roughness and circularity

579.2 HV to 560.1 HV and 126 μm to 102 μm, respectively (Fig. 10a and b). A lower N between the nozzle and workpiece enhances cooling efficiency, leading to a reduction in friction. The material compression is easily performed; thus higher hardness and depth are obtained. A higher N reduces cooling impact, lowering Vickers hardness and depth values.

When D increases from 6 mm to 10 mm, the Vickers hardness and the depth enhance from 579.2 HV to 593.3 HV and 126 μm to 158 μm, respectively (Figs. 10a and c). An increased D improves cooling efficiency at the interfaces; thus higher values of the Vickers hardness and depth are obtained.

When the Q increases from 8 L/min to 12 L/min, the Vickers hardness and depth reduce from 579.2 HV to 594.8 HV and 126 μm to 168 μm, respectively (Figs. 10a and d). A higher amount of liquid CO_2 reduces the friction at the interfaces; thus material compression is easily performed. A higher degree of plastic deformation is obtained, leading to higher Vickers hardness and depth.

Table 7. ANOVA results for the circularity model

So	SS	MS	F value	p-value
Model	349.51	38.83	26.80	< 0.0001
N	42.90	42.90	62.17	< 0.0001
D	37.75	37.75	54.72	< 0.0001
Q	31.91	31.91	46.25	< 0.0001
ND	4.19	4.19	6.07	0.0006
NQ	3.46	3.46	5.01	0.0007
DQ	5.23	5.23	7.57	0.0005
N^2	12.87	12.87	18.66	0.0002
D^2	13.83	13.83	20.04	0.0001
Q^2	14.78	14.78	21.42	< 0.0001
Res.	4.85	0.69		
Cor.	354.36			
R^2 = 0.9863; Adjusted R^2 = 0.9782; Predicted R^2 = 0.9691				

3.6 Optimal Outcomes Produced by the NSGA-II

The weight values of the roughness, energy, and circularity are 0.38, 0.26, and 0.36, respectively. Fig. 11 shows the contradictory trends of the burnishing responses. As a result, the optimal N, D, and Q are 15 mm, 9 mm, and 8 L/min, respectively. At the selected solution, the roughness, energy, and circularity are reduced by 15.5 %, 2.0 %, and 38.6 %, respectively (Table 8).

It can be stated that the cryogenic internal diamond burnishing process generated a smooth surface without any morphological irregularities. The reductions in the roughness and circularity are 79.2 % and 85.2 %, respectively, compared to the pre-burnished surface (Table 9).

Table 8. Optimization results produced by by the Kriging models-NSGA II

Method	Optimization parameters			Responses			P_i
	N [mm]	D [mm]	Q [L/min]	R [μm]	E [kJ]	V [μm]	
Initial results	25	8	8	3.464	74.42	12.22	
Optimal results	15	9	8	2.926	72.91	7.50	0.7246
Reductions [%]				15.5	2.0	38.6	

Table 9. Comparisons between the initial and optimized surfaces

Method	R [μm]	C [μm]
Initial surface	14.034	50.63
Optimal surface	2.926	7.50
Reductions [%]	79.2	85.2

4 CONCLUSIONS

In the current study, the improvements in the roughness, energy, and circularity of the diamond burnishing process were obtained using optimal N, D, and Q. The Kriging and ANFIS methods were employed to develop the response models, while the CRITIC method was applied to estimate the weights. The NSGA-II and MABAC were used to generate an optimal solution. Based on the obtained results, the following conclusions have been drawn:

1. A set of trials were executed to find the accuracy of the proposed correlations. Compared to the ANFIS, the Kriging technique provided a lower error average and a better capacity to forecast the response.
2. A lower N could be used to minimize the roughness, energy, and circularity. Higher D and Q could be applied to reduce roughness and circularity. In contrast, minimal energy was achieved using the lower D and Q.
3. For the roughness and energy models, Q had the highest contribution, followed by D and N, respectively. For the circularity model, N had the highest contribution, followed by D and Q, respectively.
4. The optimal N, D, and Q were 15 mm, 9 mm, and 8 L/min, respectively. The reductions in the roughness, energy, and circularity were 15.5 %, 2.0 %, and 38.6 %, respectively.
5. The roughness, energy consumed, and circularity of the burnished hole produced by the cryogenic CO_2 are lower than the dry one.
6. The developed process and burnishing device could be utilized for various machining internal holes with different diameters.
7. The Kriging model could be used to present complicated data when deal with the diamond burnishing operation, as compared to the ANFIS.

The impacts of the cooling parameters on the surface hardness and tribological factors will be explored in future works.

References

[1] Caudill, J., Huang, B., Arvin, C., Schoop, J., Meyer, K., Jawahir, I.S. Enhancing the surface integrity of Ti-6Al-4V alloy through cryogenic burnishing. *Procedia CIRP* 13, 243-248 (2014) **DOI:10.1016/j.procir.2014.04.042**

[2] Yang, S., Dillon, O.W. Jr., Puleo, D.A., Jawahir, I.S. Effect of cryogenic burnishing on surface integrity modifications of Co-Cr-Mo biomedical alloy. *J Biomed Mater Res B* 101, 139-152 (2013) **DOI:10.1002/jbm.b.32827**

[3] Yang, S., Umbrello, D., Dillon, O.W. Jr., Puleo, D., Jawahir, I.S. Cryogenic cooling effect on surface and subsurface microstructural modifications in burnishing of Co-Cr-Mo biomaterial. *J Mater Process Tech* 217 211-221 (2015) **DOI:10.1016/j.jmatprotec.2014.11.004**

[4] Huang, B., Kaynak, Y., Sun, Y., Jawahir, I.S. Surface layer modification by cryogenic burnishing of Al 7050-T7451 alloy and validation with FEM-based burnishing model. *Procedia CIRP* 31 1-6 (2015) **DOI:10.1016/j.procir.2015.03.097**

[5] Tang, J., Luo, H., Qi, Y., Xu, P., Ma, S., Zhang, Z. et al. The effect of cryogenic burnishing on the formation mechanism of corrosion product film of Ti-6Al-4V titanium alloy in 0.9% NaCl solution. *Surf Coat Tech* 345 123-131 (2018) **DOI:10.1016/j.surfcoat.2018.03.102**

[6] Tang, J., Luo, H.Y., Zhang, Y.B. Enhancing the surface integrity and corrosion resistance of Ti-6Al-4V titanium alloy through cryogenic burnishing. *Int J Adv Manuf Tech* 88, 2785-2793 (2017) **DOI:10.1007/s00170-016-9000-y**

[7] Sachin, B., Narendranath, S., Chakradhar, D. Enhancement of surface integrity by cryogenic diamond burnishing toward the improved functional performance of the components. *J Braz Soc Mech Sci* 41, 396 (2019) **DOI:10.1007/s40430-019-1918-1**

[8] Sachin, B., Narendranath, S., Chakradhar, D. Application of desirability approach to optimize the control factors in cryogenic diamond burnishing. *Arab J Sci Eng* 45, 1305-1317 (2019) **DOI:10.1007/s13369-019-04326-3**

[9] Rotella, G., Rinaldi, S., Filice, L. Roller burnishing of Ti6Al4V under different cooling/lubrication conditions and tool design: Effects on surface integrity. *Int J Adv Manuf Tech* 106, 431-440 (2020) **DOI:10.1007/s00170-019-04631-z**

[10] Rotella, G., Caruso, S., Del Prete, A., Filice, L. Prediction of surface integrity parameters in roller burnishing of Ti6Al4V. *Metals-Basel* 10 1671 (2020) **DOI:10.3390/met10121671**

[11] Sachin, B., Charitha, M.R., Naik, G., Puneet, N.P. Influence of slide burnishing process on the surface characteristics of precipitation hardenable steel. *SN Appl Sc* 3 223 (2021) **DOI:10.1007/s42452-021-04260-w**

[12] Caudill, J., Schoop, J., Jawahir, I.S. Correlation of surface integrity with processing parameters and advanced interface cooling/lubrication in burnishing of Ti-6Al-4V alloy. *Adv Mater Process Tech* 5 53-66 (2019) **DOI:10.1080/2374068X.2018.1511215**

[13] Huang, B., Kaynak, Y., Sun, Y., Khraisheh, M.K., Jawahir, I.S. Surface layer modification by cryogenic burnishing of Al 7050-T7451 alloy with near ultra-fine grained structure. *J Manuf Sci E-T ASME* 144 031002 (2022) **DOI:10.1016/j.procir.2015.03.097**

[14] Maximov, J., Duncheva, G., Anchev, A., Dunchev, V., Anastasov, K., Argirov, Y. Sustainable diamond burnishing of Chromium-Nickel austenitic stainless steels: Effects on Surface Integrity and Fatigue Limit. *Appl Sci-Basel* 14, 9031 (2024) **DOI:10.3390/app14199031**

[15] Van, A.L., Nguyen, T.T. Machine learning-based optimization of diamond burnishing parameters in terms of energy efficiency and quality indexes. *Arab JSci Eng* (2024) **DOI:10.1007/s13369-024-09449-w**

[16] Maximov, J., Duncheva, G., Anchev, A., Dunchev, V., Argirov, Y. Improvement in fatigue strength of Chromium-Nickel austenitic stainless steels via diamond burnishing and subsequent low-temperature gas nitriding. *Appl Sci-Basel* 14, 1020 (2024) **DOI:10.3390/app14031020**

[17] Gao, J., Wu, Y., Shen, T. On-line statistical combustion phase optimization and control of SI gasoline engines. *Appl Therm Eng* 112, 1396-1407 (2017) **DOI:10.1016/j.applthermaleng.2016.10.183**

[18] Kılavuz, F., Goren Kiral, B. Design optimization of mechanical valves in dishwashers based on the minimization of pressure losses. *Strojn vest-J Mech E* 70 194-208 (2024) **DOI:10.5545/sv-jme.2023.768**

[19] Deang, Y., Qui, L, Shao, Y., Yao, Y. Process modeling and optimization of anaerobic co-digestion of peanut hulls and swine manure using response surface methodology. *Energ Fuel* 33 11021-11033 (2019) **DOI:10.1021/acs.energyfuels.9b02381**

[20] Zhao, L. C, He, Y., Deng, X., Xia, X. H., Liang, J., Yang, G. L.; Li, W., Wang, H. Ultrasound-assisted extraction of syringin from the bark of ilex rotunda thumb using response surface methodology. *Int J Mol Sci* 13 7607-7616 (2012) **DOI: 0.3390/ijms13067607**

[21] Diakoulaki, D., Mavrotas, G., Papayannakis, L. Determining objective weights in multiple criteria problems: The critic method. *Comput Oper Res* 22 763-770 (1995) **DOI:10.1016/0305-0548(94)00059-H**

[22] Sathiya, P., Panneerselvam, K., Soundararajan, R. Optimal design for laser beam butt welding process parameter using artificial neural networks and genetic algorithm for super austenitic stainless steel. *Opt Laser Technol* 44, 1905-1914 (2012) **DOI:10.1016/j.optlastec.2012.01.025**

[23] Feng, Y., Shi, X.J., Lu, X.Q., Sun, W., Liu, K.P., Fei, Y.F:. Predictions of friction and wear in ball bearings based on a 3D point contact mixed EHL model. *Surf Coat Technol* 502 131939 **DOI:10.1016/j.surfcoat.2025.131939**

[24] Zheng, L., Zhu, Y., Zhou, Y. Meta-transfer learning-based method for multi-fault analysis and assessment in power system. *Appl Intell* 54 12112-12127 (2024). **DOI:10.1007/s10489-024-05772-9**

[25] Zhu, Y., Zhou, Y., Yan, L., Li, Z., Xin, H., Wei, W. Scaling graph neural networks for large-scale power systems analysis: Empirical laws for emergent abilities. *IEEE Trans Power Syst* 39 7445-7448 (2024) **DOI:10.1109/TPWRS.2024.3437651**

[26] Gao, D., Liu, S., Gao, Y., Li, P., Zhang : H., Wang, M A comprehensive adaptive interpretable Takagi-Sugeno-Kang fuzzy classifier for fatigue driving detection. *IEEE T Fuzzy Syst* 33 108-119 (2025) **DOI:10.1109/TFUZZ.2024.3399400**

[27] Rodić, D., Gostimirović, M., Sekulić, M., Savković, B., & Aleksić, A. Fuzzy logic approach to predict surface roughness in powder mixed electric discharge machining of Titanium Alloy. *Stroj Vestn-J Mech E* 69 376-387 (2023) **DOI:10.5545/sv-jme.2023.561**

[28] Esmaeili, M., Osanloo, M., Rashidinejad, F., Bazzazi, A.A., Taji, M. Multiple regression, ANN and ANFIS models for prediction of backbreak in the open pit blasting. *Eng Comput* 30 549-558 (2014) **DOI:10.1007/s00366-012-0298-2**

[29] Chen, J., Wang, Y., Zhang, Y., Lu, Y., Shu, Q., Hu, Y. Extrinsic-and-intrinsic reward-based multi-agent reinforcement learning for multi-UAV cooperative target encirclement. *IEEE T Intell Transp* (2024) **DOI:10.1109/TITS.2024.3524562**

[30] Tabari, M.M.R., Soltani, J. Multi-objective optimal model for conjunctive use management using SGAs and NSGA-II models. *Water Resour Manag* 27 37-53 (2013) **DOI:10.1007/s11269-012-0153-7**

[31] Miler, D., Birt, D., Hoić, M. Multi-objective optimization of the chebyshev lambda mechanism. *Stroj Vestn-J Mech E* 68 725-734 (2023) **DOI:10.5545/sv-jme.2022.349**

[32] Yao, Y., Sheng, H., Luo, Y., He, M., Li, X., Zhang, H., He, W., An, L. Optimization of anaerobic co-digestion of Solidago canadensis L. biomass and cattle slurry. *Energy* 78 122-127 (2014) **DOI:10.1016/j.energy.2014.09.013**

[33] Gao, J., Liu, A., Yang, J., Zhao, S., Liu, J. Optimization of outer-rotor flux-switching permanent magnet motor using response surface method. *Stroj Vestn-J Mech E* 70 543-553 (2024) **DOI:10.5545/sv-jme.2023.859**

[34] Pamučar, D., Ćirović, G. The selection of transport and handling resources in logistics centers using multi-attributive border approximation area comparison (MABAC). *Expert Syst Appl* 42 3016-3028 (2015) **DOI:10.1016/j.eswa.2014.11.057**

Authors Contributions *Trung-Thanh Nguyen: conceptualization, methodology, validation, writing – original draft, writing – review & editing; Minh-Thai Le: conceptualization, methodology, validation, writing – original draft, writing – review & editing; Thai-Chung Nguyen: conceptualization, methodology, validation, writing – original draft, writing – review & editing; Truong-An Nguyen: conceptualization, methodology, validation, writing – original draft, writing – review & editing; Xuan-Ba Dang: conceptualization, methodology, validation, writing – original draft, writing – review & editing; An-Le Van: conceptualization, methodology, validation, writing – original draft, writing – review & editing. All authors have read and agreed to the published version of the manuscript.*

Primerjava in optimizacija parametrov glajenja pri različnih pogojih obdelave

Povzetek Ta raziskava predlaga postopek kriogenega diamantnega glajenja in optimizira parametre hlajenja, kot so razdalja do šobe (N), premer šobe (D) in pretok CO_2 (Q), z namenom minimiziranja maksimalne hrapavosti (R), rabe energije (E) in krožnosti (C). Za izdelavo odzivnih modelov sta bili uporabljeni metodi Kriging in ANFIS (adaptive-network-based fuzzy inference system). Za izračun uteži, generiranje izvedljivih rešitev in izbiro optimalnih podatkov pa so bile uporabljene metode CRITIC, nedominirana sortirna genetska optimizacija NSGA-II in metoda MABAC. Rezultati so pokazali, da optimalne vrednosti parametrov N, D in Q znašajo 15 mm, 9 mm oziroma 8 L/min. Zmanjšanje hrapavosti, energije in krožnosti je bilo 15,5 %, 2,0 % oziroma 38,6 %. Na modela hrapavosti in energije so najbolj vplivali parametri Q, D in N, medtem ko je bil na model krožnosti vpliv parametrov N, D in Q. Predlagan postopek se lahko uporablja za obdelavo različnih lukenj ob zmanjšanem vplivu na okolje. Z uporabo kriogenega diamantnega glajenja smo dosegli manjšo hrapavost in krožnost. Kriging-NSGA-II se je izkazal kot učinkovit za prikaz nelinearnih podatkov in doseganje najboljših rezultatov.

Ključne besede kriogeno diamantno glajenje, raba energije, maksimalna hrapavost, krožnost, Kriging model